

# PHOTOMASK

BACUS—The international technical group of SPIE dedicated to the advancement of photomask technology.

PUV19 - Photonics Best Student Oral Finalist

## Pattern dependent distortion and temperature variation in EUV mask

Chung-Hyun Ban, Eun-Sang Park, Ui-Jeong Ha, Chae-Yun Lim, and Hye-Keun

Oh, Department of Applied Physics, Lithography Laboratory, Hanyang University, Korea

### ABSTRACT

Extreme ultraviolet lithography (EUVL) uses reflective optics due to the high absorption of EUV sources, and EUV masks consist of multiple layers of composites to increase reflectance. As repeated exposure proceeded, heat accumulation due to energy absorption and resulting heat deformation were observed in each layer constituting the EUV mask. In particular, the absorber is made of a material with high absorption rate, so the temperature accumulation and deformation are different depending on the part with and without the absorber. This means that thermal distortion can cause mask overlay and local critical dimension uniformity (LCDU) problems, resulting in lower process yields. In this paper, we will examine the temperature accumulation and heat deformation depending on the presence of absorber when electrostatic chuck (ESC) and hydrogen cooling are applied.

### 1. Introduction

Semiconductor manufacturing processes using extreme ultraviolet (EUVL) have reached high volume manufacturing (HVM). Nevertheless, much effort is still needed to achieve high yields. Due to the high absorptivity of EUV source, thermal deformation can occur in the mask as well as in mirrors, pellicles, and wafers.<sup>1-3)</sup> Thermal and structural deformation of EUV mask during the exposure process can be an important issue since these masks are subject to strict image placement and flatness variations. EUV masks are composed of complex layered structures, which absorb energy from each layer during exposure, increasing the temperature of the mask. This can lead to thermomechanical deformation, which can lead to poor pattern quality.<sup>4-6)</sup> The use of low thermal expansion material (LTEM) helps releasing the absorbed thermal energy, but since it cannot be completely eliminated, electrostatic chuck (ESC) and hydrogen cooling are used to keep the temperature of the mask constantly low.<sup>7-11)</sup> Despite these efforts, there may still be overlay issues and local critical dimension uniformity (LCDU) issues with regard to pattern density. We commenced this study to investigate how the mask is deformed with the pattern variation by the EUV light source and how it affects the image at the wafer. All studies were conducted through simulations. Figure 1 illustrates the research method. First, we developed a simulation model to reflect the actual exposure process conditions. Second, finite element method (FEM) analysis with appropriate boundary conditions is applied to this model. The solution of the governing differential equation for temperature accumulation and deformation of the

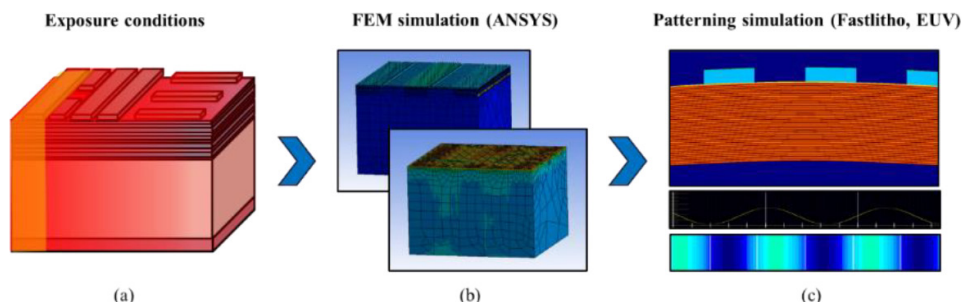


Figure 1. (a) The yellow exposure area (slit) in the EUV mask structure is scanned in the horizontal direction. (b) The front figure shows the calculated temperature change and the rear figure shows the calculated deformation. (c) Aerial image example by modeling the mask deformation that occurs in the commercial lithography tool, FastLitho.

BACUS  
N • E • W • S

AUGUST 2020  
VOLUME 36, ISSUE 8

TAKE A LOOK  
INSIDE:

INDUSTRY BRIEFS  
—see page 9

CALENDAR  
For a list of meetings  
—see page 10

SPIE.

# EDITORIAL

## Masks can save lives from COVID-19

**Tony Vacca**, Automated Visual Inspection

The current emphasis is for everyone to use masks to curb the COVID-19 pandemic. Our relatively small photomask community has known for years the critical role masks play in the fabrication of electronic health care devices. With the current pandemic, everyone is talking about the importance and life-saving abilities of using masks. Many people are wearing masks with prints on the fabric which by default, makes it a photomask. It is about time masks finally get the recognition they deserve!

On a serious note, the semiconductor industry has provided faster, and cheaper devices which has enabled major advancements in the medical industry. Virtually all medical equipment now uses semiconductor chips including ventilators, heart monitors, and even thermometers which are now digital, more accurate, and faster than its predecessor (mercury in a vacuum). In fact, the latest thermometers used in COVID-19 testing facilities send immediate results via Bluetooth/internet to the local health officials enabling real-time data analysis!

Necessity is the mother of invention. Entrepreneurs have recently discovered a very inexpensive way to clean masks using an everyday multicooker <https://www.dhs.gov/publication/st-multicooker-decontamination-n95-respirators>. I believe we should investigate this low-cost technology as an alternative to our current mask cleaning methods.

During these tumultuous times, I hope we can all agree that masks are proven to be critical in the treatment and the defense of disease spread.

Make a mask, keep it clean, and use it!

Stay safe my friends

**Caution: Please refrain from using a pellicle on the mask for your face. It tends to impede airflow which has been proven to be helpful for human life.**



N • E • W • S

BACUS News is published monthly by SPIE for BACUS, the international technical group of SPIE dedicated to the advancement of photomask technology.

**Managing Editor/Graphics** Linda DeLano

**SPIE Sales Representative, Exhibitions, and Sponsorships**  
Melissa Valum

**BACUS Technical Group Manager** Marilyn Gorsuch

### ■ 2020 BACUS Steering Committee ■

#### President

**Peter D. Buck**, *Mentor Graphics Corp.*

#### Vice-President

**Emily E. Gallagher**, *imec*

#### Secretary

**Kent Nakagawa**, *Toppa Photomasks, Inc.*

#### Newsletter Editor

**Artur Balasinski**, *Cypress Semiconductor Corp.*

#### 2020 Photomask + Technology Conference Chairs

**Moshe Preil**, *KLA-Tencor Corp.*

**Stephen P. Renwick**, *Nikon Research Corp. of America*

#### International Chair

**Uwe F. W. Behringer**, *UBC Microelectronics*

#### Education Chair

**Frank E. Abboud**, *Intel Corp.*

#### Members at Large

**Michael D. Archuletta**, *RAVE LLC*

**Brian Cha**, *Samsung Electronics Co., Ltd.*

**Thomas B. Faure**, *GLOBALFOUNDRIES Inc.*

**Aki Fujimura**, *DS2, Inc.*

**Brian J. Grenon**, *Grenon Consulting*

**Jon Haines**, *Micron Technology Inc.*

**Naoya Hayashi**, *Dai Nippon Printing Co., Ltd.*

**Bryan S. Kasproicz**, *Photronics, Inc.*

**Romain J. Lallement**, *IBM Research*

**Patrick M. Martin**, *Applied Materials, Inc.*

**Jan Hendrik Peters**, *bmbg consult*

**Jed Rankin**, *GLOBALFOUNDRIES Inc.*

**Douglas J. Resnick**, *Canon Nanotechnologies, Inc.*

**Thomas Scheruebl**, *Carl Zeiss SMT GmbH*

**Thomas Struck**, *Infineon Technologies AG*

**Bala Thumma**, *Synopsys, Inc.*

**Anthony Vacca**, *Automated Visual Inspection*

**Vidya Vaenkatesan**, *ASML Netherlands BV*

**Michael Watt**, *Shin-Etsu MicroSi Inc.*

**Larry Zurbrick**, *Keysight Technologies, Inc.*

## SPIE.

P.O. Box 10, Bellingham, WA 98227-0010 USA

Tel: +1 360 676 3290

Fax: +1 360 647 1445

SPIE.org

help@spie.org

©2020

All rights reserved.

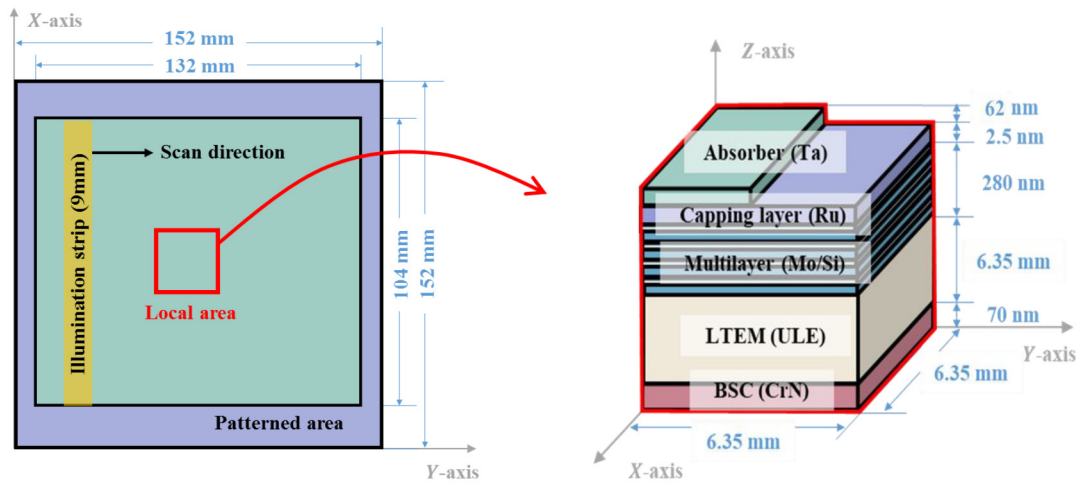


Figure 2. Schematic of the modeled EUV mask structure.

Table 1. Physical properties of EUV mask materials.

Property	Tantalum	Nickel	Ruthenium	Silicon	Molybdenum	LTEM
Density ( $\text{g}\cdot\text{cm}^3$ )	16.69	8.91	12.45	2.33	2.21	2.21
Thermal expansion coefficient ( $1/\text{K}$ )	$6.3\times 10^{-6}$	$1.1\times 10^{-5}$	$6.4\times 10^{-6}$	$2.56\times 10^{-6}$	$4.8\times 10^{-8}$	$0.3\times 10^{-8}$
Reference temperature (K)	300	300	300	300	300	300
Young's modulus ( $\text{Pa}$ )	$1.86\times 10^{11}$	$2.00\times 10^{11}$	$4.47\times 10^{11}$	$1.50\times 10^{11}$	$3.29\times 10^{11}$	$6.76\times 10^{10}$
Poisson's ratio	0.34	0.31	0.30	0.17	0.31	0.17
Thermal conductivity ( $\text{W}/\text{m}\cdot\text{K}$ )	57.5	90.9	117	149	138	1.31
Specific heat ( $\text{J}/\text{kg}\cdot\text{K}$ )	139	440	238	0.71	0.25	767
Emissivity	0.14	0.03	0.34	0.83	0.08	0.82
Complex refractive index at EUV	0.0330	0.1556	0.0127	0.0018	0.0064	0.0108

EUV mask with repeated exposures is obtained. Third, we examined how thermal deformation of masks affects the image using commercial photolithography tools. Due to the nature of computer simulations, it is not possible to reflect all of the actual exposure conditions. Therefore, we have created a simple model by selecting effects that can have a significant impact on the actual exposure process. The simulation model uses transient thermal modules from ANSYS®, a finite element analysis tool based on thermal equations.<sup>12)</sup>

## 2. Development of a Reasonable Computer Simulation Model

### 2.1 Modeling process

EUV masks consist of multilayer thin films such as anti-reflective coating (ARC), absorber, capping layer, Mo/Si layer and LTEM. In general, EUV mask comprises of 2 nm antireflective coating, 60 nm absorber, 2.5 nm capping layer, 280 nm multilayer (40 pairs of 4.2 nm Mo and 2.8 nm Si), 6.35 mm LTEM, and 70 nm back side coating (BSC).<sup>13)</sup> We have developed a model with this following structure. Anti-reflection coating with tantalum oxide, absorber with tantalum, capping layer with ruthenium, and back side coating (BSC) with chromium were used. LTEM was tested with quartz, pyrex, ULE, and zerodur, and the ULE was used because of its low thermal expansion coefficient and low stress. The area of commercial EUV masks uses an area of 132 Å-104 mm<sup>2</sup> out of the total area of 152 Å-152 mm<sup>2</sup>.<sup>14,15)</sup> In order to ensure computational efficiency, the EUV mask

size of 6.35 Å-6.35 mm<sup>2</sup> was considered, assuming a symmetrical pattern.

There are many different types of ESCs used for fixing EUV masks, emitting electrons and reducing temperature accumulation. The simulation uses a dielectric chuck with a 15 mm ULE body covered with an Al<sub>2</sub>O<sub>3</sub> 0.2 mm dielectric film. Each material was taken into account density, CTE, Young's modulus, Poisson's ratio, thermal conductivity, specific heat, emissivity, and  $k$  values as shown in Table 1 for effective temperature accumulation and thermal deformation calculations.

In consideration of the accuracy and efficiency of the calculation, 30,000 elements per model with 200,000 nodes, and time step of 10-3s are applied on average. EUV masks are repeatedly exposed by scanning method.<sup>16-19)</sup> EUV masks were modeled using three-dimensional solid elements.<sup>20-22)</sup> Table 3 shows estimated values of exposure per die, die alignment time, and wafer alignment time based on the source power, throughput, number of dies, and scan speed of the latest ASML NXE 3400B model. For instance, 0.11 s exposure on a 132 mm mask, so 6 mm slit is exposed 0.01 s and exposed again after 0.22 s. and a new exposure starts after 6.5 s after all dies have been exposed. Initial temperature starts at 300 K. In the structural analysis, the bottom of the ESC was assumed to be fully constrained. With the exception of the ESC, the friction between the mask layers was ignored to free the expansion of mask. Radiation boundary conditions were applied to all surfaces at the top of the mask. The emissivity values used for the surface materials are listed in Table 1.

Table 2. Simulation conditions of EUV mask model.

Parameter	Values
Volume ( $\text{mm}^3$ )	$6.35 \times 6.35 \times 21.55$
Materials	ULE, Al, Cr, Mo, Si, Ru, Ta
Exposure time (s)	1
Contacts	Slider 100
Mesh	Relevance 100
Mesh type	Hex dominant method
Nodes	(average) 200,000
Elements	(average) 30,000
Initial Temperature (K)	300
Time step (s)	$10^{-3}$

Table 3. Physical properties of EUV mask materials.

Parameter	Values
Scanning process	Considered
Source power (W)	250
Heat flux ( $\text{W}/\text{cm}^2$ )	5
Throughput (wph)	125
Fields per wafer (shots)	96
Illumination field width (mm)	6
Scan velocity ( $\text{mm}/\text{s}$ )	300
Illumination time per die (s)	0.11
Die align time (s)	0.12
Wafer align time (s)	6.50

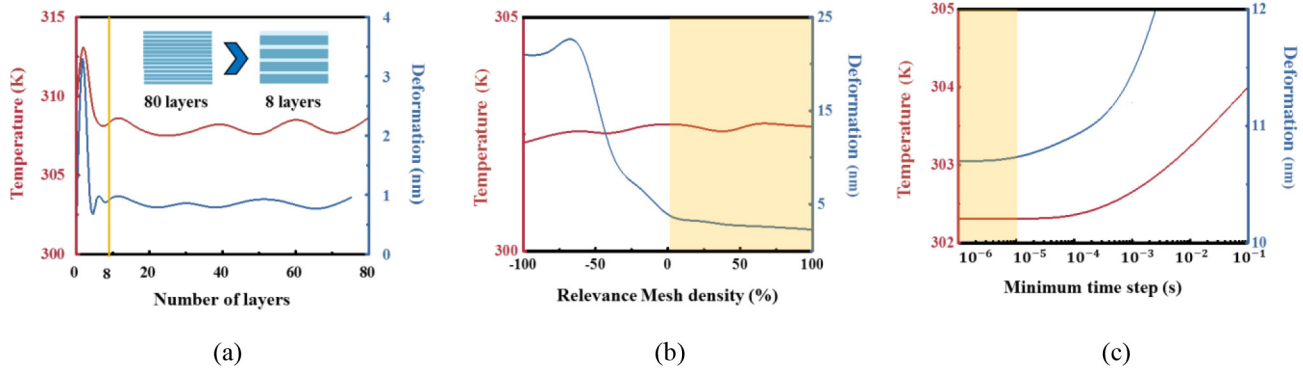


Figure 3. (a) Temperature and deformation variations as the number of film layer changes. (b) Dependence of the FEM calculation results for temperature on mesh relevance. (c) Convergence as a function of time step in the FEM model.

## 2.2 Optimization

Incorrect settings can result in meaningless calculations. Generally, model with good conditions will yield accurate results. However, much more complex models can be computationally unsuccessful or can take too long to calculate. Therefore, proper optimization is required. In FEM simulations, the accuracy and calculation speed are significantly dependent on the structure of model, contact conditions, mesh density, time step, and boundary conditions. Figure 3(b) shows an example of how mesh optimization affects accuracy. Mesh relevance is related to how complicated the calculation is. As the mesh relevance approaches 100%, more accurate values are obtained. However, depending on the situation, calculations may take a significant amount of time to complete. Conversely, more inaccurate results are obtained when the mesh relevance is closer to -100%. Therefore, we need to find a condition that is accurate within a valid range with the best computational efficiency.

First, we considered the proper model structure. We assumed that the symmetric pattern structure was repeated throughout the mask prior to simulation for complex patterning. By calculating the volume of the local area instead of the entire mask, we were able to quickly observe the thermodynamic behavior of the mask and the tendencies of the absorber variations. For the same reason, we considered simpler structures than actual masks. The EUV mask is composed of LTEM, multilayer, capping layer and absorber. The multilayer is composed of 40 thin film pairs. We first modeled the EUV mask structure with 80 layers. Table 2 shows the concrete simulation condition used in this model. The contact condition which is a setting in the simulation program is slider 100. The contact condition defines how the calculation network is shared. This slider setting forces layers of the same species share a computation node and have clear contact with the other surface. The mesh type uses the hex dominant calculation method for the mask. This increases the speed of the system by appropriately reflecting that the scale of LTEM is much larger than those of the absorber, capping layer, and multilayer, and that

the heat flux absorbed toward the bottom of the LTEM decreases. ULE, Mo/Si, Ru, and Ta were used as the LTEM, multilayer, capping layer, and absorber materials, respectively. Table 1 contains the physical properties of materials used in the simulation.<sup>23)</sup> We checked the temperature change and deformation of the mask by reducing the number of multilayers. Temperature and deformation variations are not much changed with number of layers are reduced to 8 (Figure 3(a)). To ensure the computational efficiency and consistency, the number of layers in the multilayer film was reduced from 80 to 8. This may cause problems in actual EUVL due to low reflectance, however the thermomechanical effect was very small, within the error range.

Second, technical optimization was performed in ANSYS®. Figure 3(b) and (c) show the simulated temperature and deformation results with mesh and time step. The FEM calculation results for temperature and deformation depend on the mesh density (Figure 3(b)). In particular, the solution to mask deformation highly depends on mesh density. Tighter meshes make calculations more difficult, but calculation accuracy increases. Since mesh relevance showed a tendency to converge to deformations at more than 0%, we have achieved accuracy and efficiency of computation using mesh relevance greater than 0%. The minimum calculation time unit is also important in FEM simulation (Figure 3(c)). Time-varying models require computer simulation with transient modules. The time step represents how closely the time interval is calculated. Likewise, smaller time steps require greater computational power and yield more accurate results. In particular, the mask deformation solution is sensitive to calculation time. This trade-off relationship requires optimization. We used a minimum time step with  $10^{-3}$  s.

## 2.3 Verifying the consistency of the simulation models

Before performing simulations of concrete models, it is necessary to check whether the developed models yield a reasonable result. We have confirmed that the results of computational simulation are consistent with calculated results using theoretical formulas. The simplest models

were considered when investigating and confirming consistency. Instead of the complex EUV mask model, we considered a LTEM monolayer, which occupies the largest volume in the EUV mask. We considered an effective full-area exposure that gives similar results rather than a scan exposure. The exposed mask area was  $132 \times 104 \text{ mm}^2$  in this simulation. We confirmed the model consistency by comparing four models with various LTEM thicknesses of 6.25 mm, 62.5  $\mu\text{m}$ , 6.25  $\mu\text{m}$ , and 62.5 nm. The basic thermodynamic equation (Eq. (1)) was used in a simple thermal equation of LTEM (Eq. (2)). This system was numerically solved and compared with the results from simulations.

$$Q = \alpha \cdot P \cdot \Delta t = c \cdot m \cdot \Delta T \quad (1)$$

$$\frac{dT}{dt} = \frac{1}{c \cdot m} \frac{dQ}{dt} = \frac{1}{c \cdot m} \cdot [\alpha \cdot P - \varepsilon \cdot \sigma \cdot S \cdot (T^4 - T_s^4)] \quad (2)$$

$Q$  is the total heat,  $\alpha$  is the absorption ratio,  $P$  is the EUV beam power,  $\Delta t$  is the exposure time,  $\Delta T$  is the change in temperature,  $c$  is the specific heat,  $m$  is the LTEM mass,  $\varepsilon$  is the emissivity,  $\sigma$  is the Boltzmann constant ( $=5.67 \times 10^{-8} \text{ W/m}^2\text{K}$ ),  $S$  is the radiating surface area,  $T_s$  is the ambient temperature, and  $T$  is the accumulated temperature during exposure. The most basic thermodynamic equation (Eq. (1)) does not consider cooling by conduction, convection or radiation.<sup>24,25</sup> Since EUVL is performed in a vacuum, convection is not considered in the simple thermal equation describing the LTEM. Conduction along the thickness direction is thin and is ignored. Since thermal radiation emits from the front and back sides of the thin film,  $S$  is twice the total thin film area. We numerically solved this equation and compared it with simulation results. The specific simulation conditions are specified in Table 2. ULE was used as the LTEM material, since ULE showed better thermal properties than other materials due to its low thermal expansion coefficient among the various quartz-based LTEM candidate materials. We verified the temperature variation according to the LTEM thickness. The FEM simulation results and analytic calculations of the theoretical formulas are indicated with solid and dotted lines in Figure 4, respectively. The results from the FEM simulation and numerical analysis are almost identical.

### 3. Thermal Variation and Deformation with Various Models

#### 3.1 Temperature and deformation according to mask structure

Before examine the temperature accumulation and deformation according to the pattern, we examined at the difference in temperature accumulation by stacking each layer that constitutes the EUV mask to check how the temperature change depends on the presence or absence of an absorber. Using the simulation conditions described in Tables 2 and 3, accumulated temperature and deformation along the mask structure were investigated. Figure 6 shows the result of temperature accumulation as we stack each layer that makes up the EUV mask. 44 exposures were performed during a 10-second simulation time. In the case of the LTEM single structure, a material with a large heat capacity and a low thermal deformation was selected, which resulted in a relatively high temperature accumulation. Designed to achieve high reflectance, the multilayer has a high reflectance of 72.24% on the surface, resulting in a marked reduction in cumulative temperature. The capping layer with good emissivity and anti-oxidation has accumulated temperature similar to multilayer. The absorber uses a high absorption material to form a pattern, so the energy absorption is high and the temperature accumulation is relatively high. As will be mentioned again at the end of the paper, the absorber has a relatively large coefficient of thermal expansion, so the thermal deformation due to temperature accumulation is also relatively large. In particular, high- $k$  material absorbers intended to be used as absorbers in next-generation EUV masks exhibited greater degrees of temperature accumulation and deformation even at lower heights. It was a short time simulation of 10 s, but the change in temperature accumulation clearly shows the difference between mask structures. This is why we investigated the effects

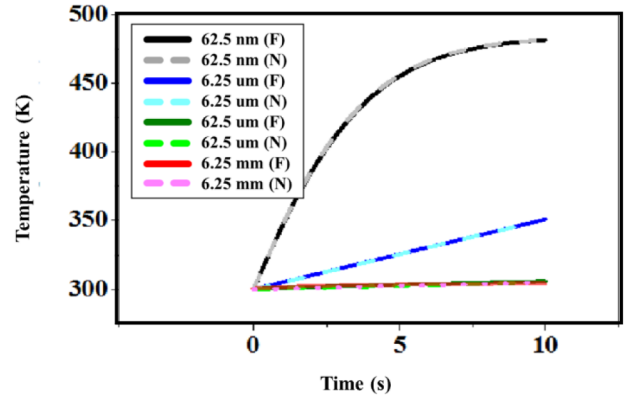


Figure 4. Simple LTEM monolayer models with varying thicknesses of 6.25 mm, 62.5  $\mu\text{m}$ , 6.25  $\mu\text{m}$ , and 62.5 nm were examined. Comparison of FEM simulation results (F) and theoretical calculations (N) shown with solid and dotted lines on the graph, respectively.

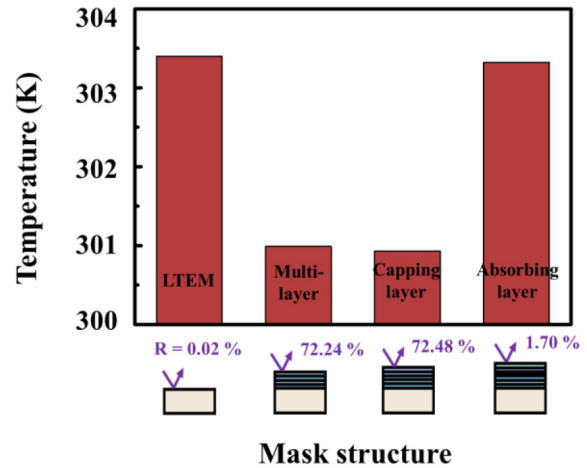


Figure 5. Accumulated temperature due to lamination of each structure in the mask.

of absorber variation.

#### 3.2 Temperature and deformation with absorber variation

Temperature accumulation was investigated during the 10 s simulation for two main examples of change in absorber thickness and change in absorber ratio per unit area. First, the difference in temperature accumulation with absorber thickness was investigated. Various absorber thickness values were applied to the model. In general, the absorber has a 2 nm thick antireflective coating and a structure with a thickness of 60 nm. Therefore, the temperature accumulation for absorber thicknesses ranging from 42 nm to 82 nm were investigated. In Figure 7, all models have a 50% absorption rate per unit area. The remaining 50% part has no absorber and the capping layer occupies the top. The green and purple lines in the graph represent the accumulated temperature result of the absorber and the capping layer without the absorber, respectively. In the region without absorber, the reflectance was fixed at 72.48%, but since the reflectance was changed from 0.09% to 3.46% depending on the height of the absorber, the temperature accumulation in the absorber area did not show a linear graph. The most popular 62 nm thick absorber layer had good absorption compared to other absorber thickness. Heat deformation is a function of temperature, but because the absorber height changes, further study is required.

Second, the difference in temperature accumulation with respect to the absorber ratio was investigated. Figure 8 shows the cumulative

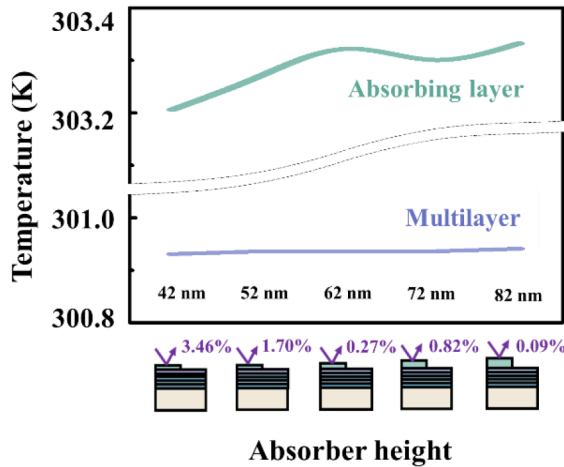


Figure 6. Temperature accumulation variation with absorber thickness: The green line in the graph represents the temperature accumulation in the absorber region and the purple line represents the temperature accumulation in the absence of the absorber region. Since the reflectance changes with the thickness of the absorber, the temperature accumulation with the absorber thickness is not linear.

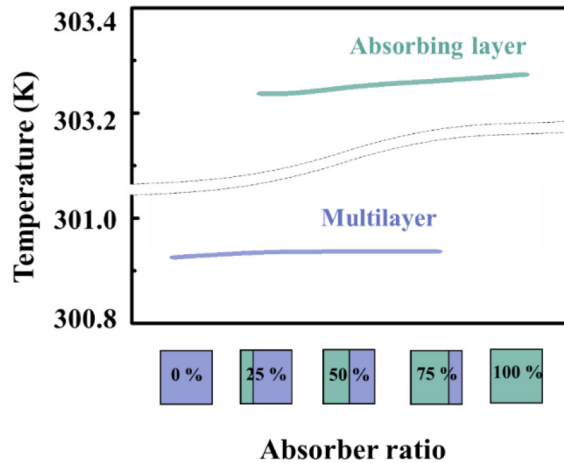


Figure 7. Temperature accumulation result according to absorber ratio: Green line shows the temperature accumulation in the absorber area and purple line shows the temperature accumulation in the area without the absorber. As the absorber ratio increased, the temperature accumulation increased in both the absorbent and nonabsorbent parts.

temperature when the ratio of absorber per unit area is from 0% (blank mask) to 100%. The green and purple lines in the graph represent the accumulated temperatures of the absorber and the capping layer without the absorber, respectively. The absorber ratio gradually increases toward the right. As the absorber ratio increased, so did the temperature accumulation. In the absence of absorbers as well as in the absorber zones, more temperatures accumulate as the absorber ratio increases. This means that as the pattern density increases, the potential for thermal deformation can increase.

### 3.3 Difference in temperature accumulation by pattern change

We looked at the degree of temperature accumulation as the pattern changes. Figure 9 shows the temperature accumulations of absorber for line and space pattern (LS) in 1:1 and 1:10 ratios for pattern sizes of 80 nm, 100 nm, and 125 nm in the mask after 10 s of simulation. LTEM

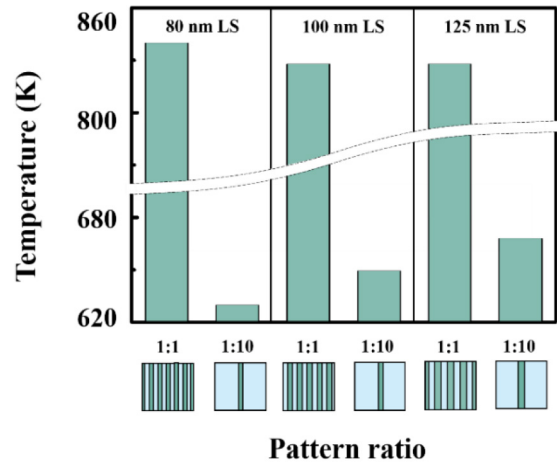


Figure 8. Cumulative temperature change according to pattern change when LTEM structure is omitted for computational efficiency: Simulation time is 10 s and green bar means absorber temperature. The smaller and denser the pattern goes the greater the temperature accumulation becomes.

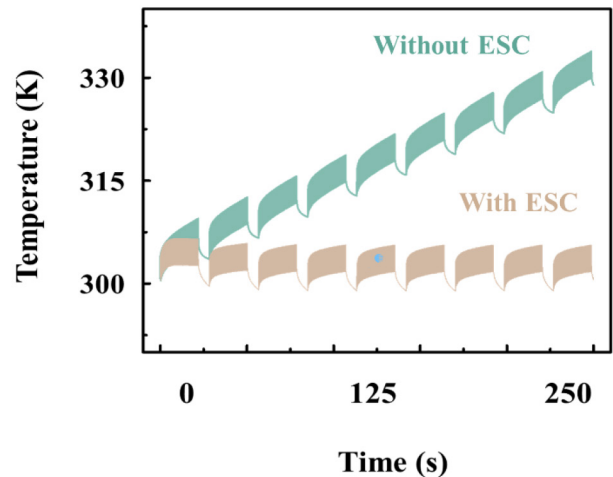


Figure 9. Temperature accumulation with and without ESC for 250 s of simulation time for LTEM single structure: LTEM temperature was decreased by ESC as exposure was repeated.

and BSC, which reduce the temperature accumulation of the mask, have been omitted to reduce the computation time, and attention should be paid to the relative temperature change according to the pattern change. The green bar graph shows the result of temperature accumulation in the absorber area. More temperature accumulation occurred in the 1:1 line & space pattern than in the 1:10 line & space pattern.

### 3.4 Temperature accumulation and deformation with ESC and hydrogen convection cooling

ESC and  $H_2$  flow cooling can be used to reduce thermal strain in these EUV masks. Temperature accumulation was examined with and without ESC, with and without hydrogen cooling, and with and without ESC and hydrogen cooling. Finally, thermal deformations with and without hydrogen cooling examined. First, we looked at the degree of temperature accumulation with and without ESC for 250 s of simulation time for the EUV mask structure. Each layer constituting the EUV mask has a thickness of a few nm for thin areas and a few mm for thick areas. Therefore, computational mesh optimization is needed. Due to computational efficiency problem, we use the local area of the EUV mask structure instead of the entire mask structure. The yellow and green lines represent the

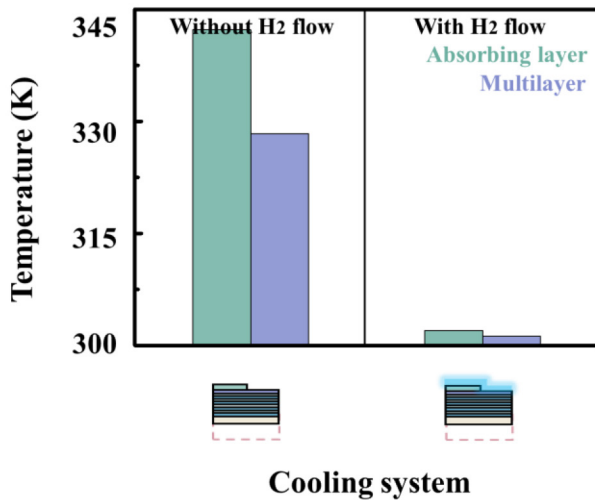


Figure 10. Cumulative difference in temperature with and without hydrogen cooling: A short simulation time of 10 s, but much heat has cooled by H<sub>2</sub> flow cooling.

temperatures of the EUV mask structure without ESC and the EUV mask structure with ESC, respectively. In the short exposure time, the cooling effect of ESC was insignificant, but as the exposure was repeated, the temperature accumulation degree of EUV mask was clearly different. At this time, the ESC remain at 295 K from the beginning to the end of the exposure due to cooling. Further studies on saturation temperature are underway when ESCs exist for the entire EUV mask structure.

Second, the temperature accumulation of EUV mask with and without the presence of convection by H<sub>2</sub> flow was examined for 10 s. The green and purple bar graphs represent the temperature of the absorbing and non-absorbing capping layers, respectively. The cooling effect of ESC was insignificant during the short exposure time of 10 s, but the temperature accumulation due to convection was relatively large. In general, the convection coefficient value is 5 ~ 10 W/m<sup>2</sup>•K for natural convection and 10 to 50 W/m<sup>2</sup>•K for forced convection. In the simulation, the temperature of hydrogen is 300 K and the convection coefficient is 1 W/cm<sup>2</sup>•K.

Third, the deformation of EUV mask was examined after 10 s of simulation depending on the presence of H<sub>2</sub> flow convection. The green and purple bar graphs show the degree of thermal deformation of the absorbing layer and nonabsorbing capping layers, respectively. The hydrogen flow cooling reduced the temperature accumulation considerably during the short exposure time of 10 s. After H<sub>2</sub> cooling, the temperature accumulation was different depending on the presence or absence of the absorber, which means that the image quality may be reduced depending on the pattern during cooling. In the simulation, the conditions for the inlet and outlet have not been specified yet, and the hydrogen flow is fixed at 300 K, resulting in a relatively low flow rate. Good use of hydrogen cooling can prevent defects between the pellicle and the mask and suppress thermal deformation of the pellicle and mask. In order to reflect the actual hydrogen cooling, literature review is ongoing, and when the forced convection is severe, we plan to check whether there is a difference in the deformation result depending on the presence of the absorber. Further research is ongoing to see how these deformation differences affect the actual wafer image.

#### 4. Conclusions

EUV photo mask distortion caused by heat can cause pattern placement errors and overlay problems, which can be a significant problem in the manufacturing process. In addition, LCDU problems caused by pattern changes can be an important issue in addition to overlay problems, as they are very difficult to correct. Distorted mask patterns are directly related to wafer image errors and can reduce process yield. The thermal

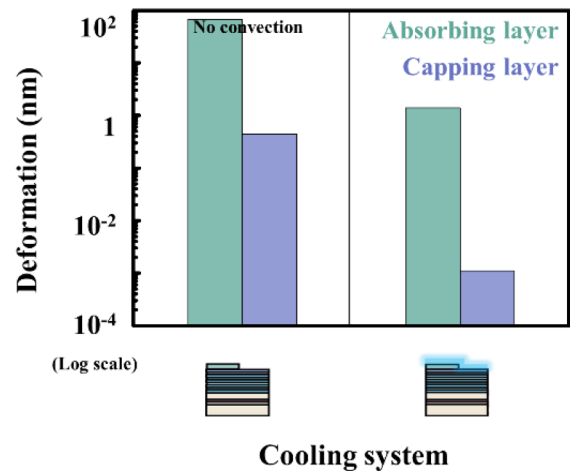


Figure 11. Deformation of EUV mask with or without H<sub>2</sub> flow convection after 10 s simulation time: Hydrogen cooling can effectively suppress thermal deformation of EUV mask, but there is still a difference of deformation with or without absorber.

deformation of EUV masks showed a large difference according to the change of absorber, and the denser the pattern, the deeper the thermal deformation. Mask cooling with ESC was effective during long exposures and cooling with hydrogen convection was immediate. However, under the conditions used for the simulation, the degree of temperature accumulation and deformation differed depending on the presence of the absorber even after such cooling, which may cause LCDU problems.

Several assumptions have been used to ensure computational efficiency in terms of consistency of results. The change in temperature of the mask was investigated using a symmetric model for the local area. Significantly reduced computational costs with a simplified model. The temperature and deformation of the mask can be affected by the mask structure and materials. Some properties which have thickness dependence used bulk values. Although the main trend is identified in this paper, further study is underway to reflect the actual process.

#### 5. Acknowledgments

This work was supported by the Future Semiconductor Device Technology Development Program #10052714 funded By MOTIE(Ministry of Trade, Industry & Energy) and KSRC(Korea Semiconductor Research Consortium).

#### 6. References

- [1] Obert Wood, Sudhar Raghunathan, Pawitter Mangat, Vicky Philipsen, Vu Luong, Patrick Kearneyd Erik Verduijn, Aditya Kumar, Suraj Patil, Christian Laubis, Victor Soltwisch and Frank Scholze, **Proc. SPIE 9422**, 942201 (2015).
- [2] T. Kamo, H. Aoyama, T. Tanaka, and O. Suga, **Proc. SPIE 6730**, 673017 (2017).
- [3] Jean Yves Robic, Patrick Schiavone, Vincent Rodillon, Renaud Payerne, *Microelectronic Eng.* 61, 257 (2002).
- [4] S. E. Gianoulakis and A. K. Ray-Chaudhuri, *Journal of Vacuum Science and Technology B* 16, 3440 (1998).
- [5] Steven E. Gianoulakis and Avijit K. Ray Chaudhurib, **Proc. SPIE 3676** (1999).
- [6] Tsutomu Shoki, Takeyuki Yamada, Shouji Shimojima, Yuuki Shiota, Mitsuharu Tsukahara, Kesahiro Koike, Hiroaki Shishido, Osamu Nozawa, Toshiyuki Sakamoto, and Morio Hosoya, **Proc. SPIE 6730**, 673015 (2007).
- [7] S. E. Gianoulakis and A. K. Ray-Chaudhuri, **Proc. SPIE 3696** (1999).
- [8] R. Engelstad, J. Sohn, A. R. Mikkelsen, M. Nataraju, and K. T. Turner, **Proc. SPIE 6730**, 673004 (2007).

- [9] Valérie Paret, Pierre Boher, Roland Geyl, Bernard Vidal, Magali Putero-Vuaroqueaux, Etienne Quesnel, and Jean Yves Robic, *Microelectronic Eng.* 61, 145 (2002).
- [10] Richard H. Stulen and Donald W. Sweeney, *IEEE* 35 (1999).
- [11] Pei-yang Yan, Michael Leeson, Sang Lee, Guojing Zhang, Eric Gullikson, and Farhad Salmassi, **Proc. SPIE** 1932 (2011).
- [12] Amr Y. Abdo, R. L. Engelstad, William A. Beckman, Edward G. Lovell, and John W. Mitchell, **Proc. SPIE** 5377, 1452 (2004).
- [13] Amr Y. Abdo, Roxann L. Engelstad, William A. Beckman, Edward G. Lovell, **Proc. SPIE** 1537, (2004).
- [14] Kevin Kemp, and Stefan Wurm, *C. R. Physique* 7, 875 (2006).
- [15] Carl J. Martin, Roxann L. Engelstad, and Edward G. Lovell, **Proc. SPIE** 4343 (2001).
- [16] Benjamin G. Eynon, and Jr, Banqiu Wu, *Photomask Fabrication Technology* (McGraw-Hill, 2005) p.261.
- [17] H. J. Levinson, *Principles of Lithography* (SPIE Press, Bellingham, 2001), p. 341.
- [18] V. Bakshi, *EUV Lithography* (SPIE Press, Bellingham, 2009), p. 42.
- [19] G. Kostovski, *Advanced in Unconventional Lithography* (InTech, Rijeka, 2011), p. 168.
- [20] Akira Chiba, Minoru Sugawara, Hiromasa Yamanashi and Iwao Nishiyama, *J. Appl. Phys.* 42, 3784 (2003).
- [21] C. Gwynn, *Extreme Ultraviolet Lithography* (A White Paper, CA, 1998).
- [22] Yanqiu Li, Zhou Pengfei, and Zhang Fei, *J. Appl. Phys.* 46, 5104 (2007)
- [23] Pei.-yang Yan, Guojing Zhang, Patrick Kofron, Jeff Powers, Mark Tran, Ted Liang, Alan Stivers, and Fu-Chang Lo, **Proc. SPIE** 4066 (2000).
- [24] Akira Chiba, Kazuya Ota, Eiichi Hoshino, Taro Ogawa and Shinji Okazaki, *J. Appl. Phys.* 41, 4091 (2002).
- [25] Carl J. Martin, Roxann L. Engelstad, and Edward G. Lovell, **Proc. SPIE** 4343 (2001).



## Sponsorship Opportunities

Sign up now for the best sponsorship opportunities

### Photomask Technology + EUV Lithography 2020

Contact: Melissa Valum

Tel: +1 360 685 5596; [melissav@spie.org](mailto:melissav@spie.org)

### Advanced Lithography 2021

Contact: Teresa Roles-Meier

Tel: +1 360 685 5445; [teresar@spie.org](mailto:teresar@spie.org)

## Advertise in the BACUS News!

The BACUS Newsletter is the premier publication serving the photomask industry. For information on how to advertise, contact:

Melissa Valum

Tel: +1 360 685 5596

[melissav@spie.org](mailto:melissav@spie.org)

## BACUS Corporate Members

Acuphase Inc.

American Coating Technologies LLC

AMETEK Precitech, Inc.

Berliner Glas KGaA Herbert Kubatz GmbH & Co.

FUJIFILM Electronic Materials U.S.A., Inc.

Gudeng Precision Industrial Co., Ltd.

Halocarbon Products

HamaTech APE GmbH & Co. KG

Hitachi High Technologies America, Inc.

JEOL USA Inc.

Mentor Graphics Corp.

Molecular Imprints, Inc.

Panavision Federal Systems, LLC

Profilocolore Srl

Raytheon ELCAN Optical Technologies

XYALIS

# Industry Briefs

## ■ EUV Lithography in Outer Space

JUNE 2ND, 2020

**MARK LAPEDUS**, Semiconductor Engineering

The U.S. space program made history on May 31, 2020, when NASA astronauts Robert Behnken and Douglas Hurley aboard SpaceX's Crew Dragon spacecraft arrived at the International Space Station (ISS). This is the first time a commercial spacecraft has delivered astronauts to the ISS.

The ISS serves as a research lab for companies, government agencies and universities. Recently, the world's first EUV-based experiment was successfully conducted on the ISS, which could lay the foundation for manufacturing in space. The materials from Astrileux could enable a new class of instruments. It also lays the foundation for EUV-based lithography in space, which use the power of solar radiation as the light source.

<https://semiengineering.com/manufacturing-bits-june-2-2/>

## ■ Japanese Companies Fight for Share of EUV Chip Technology Sector

July 12, 2020

**YOICHIRO HIROI**, Nikkei staff writer, Nikkei Asia Review

TOKYO -- EUV is the focus of competition among Japanese equipment manufacturers including Tokyo Electron and Lasertec. The ongoing generational change involving technological advances in the equipment market is worth more than 6 trillion yen (\$56.5bn) annually and is generating a huge impact.

<https://asia.nikkei.com/Business/Electronics/Japanese-companies-fight-for-share-of-EUV-chip-technology-sector>

## ■ Nvidia's Market Value Bigger Than Intel

July 10, 2020

**Sally Ward-Foxton**, EE Times

Nvidia's market value has grown bigger than chip giant Intel's for the first time, reaching \$251 billion; 79% year-to-date, while Intel stock has fallen 2.4% over the same period. Nvidia's market value makes it the third-largest semiconductor company today, behind TSMC and Samsung.

Nvidia reached this milestone following excellent Q1 growth (for first quarter ended April 26, 2020), reported last month — first-quarter revenues were \$3.08 billion, up 39% from a year earlier but down 1% sequentially.

<https://www.eetimes.com/nvidias-market-value-bigger-than-intel/>

## ■ DNP Develops Photomask Process Targeting 5nm EUV Lithography

July 14, 2020, EE Times Japan

Dai Nippon Printing Co., Ltd. (DNP) announced the development of a photomask process capable of accommodating 5nm EUV lithography, with the multi-beam mask writing tool (MBMW) by DNP in 2016.

DNP will provide photomasks for EUV lithography and will support development relating to EUV lithography. It targets sales of 6 billion yen per year in FY 2023.

[https://headlines.yahoo.co.jp/hl?a=20200714-00000091-it\\_eetimes-ind](https://headlines.yahoo.co.jp/hl?a=20200714-00000091-it_eetimes-ind)  
[https://www.dnp.co.jp/eng/news/detail/10158438\\_2453.html](https://www.dnp.co.jp/eng/news/detail/10158438_2453.html)

# Join the premier professional organization for mask makers and mask users!

## About the BACUS Group

Founded in 1980 by a group of chrome blank users wanting a single voice to interact with suppliers, BACUS has grown to become the largest and most widely known forum for the exchange of technical information of interest to photomask and reticle makers. BACUS joined SPIE in January of 1991 to expand the exchange of information with mask makers around the world.

The group sponsors an informative monthly meeting and newsletter, BACUS News. The BACUS annual Photomask Technology Symposium covers photomask technology, photomask processes, lithography, materials and resists, phase shift masks, inspection and repair, metrology, and quality and manufacturing management.

### Individual Membership Benefits include:

- Subscription to BACUS News (monthly)
- Eligibility to hold office on BACUS Steering Committee

[spie.org/bacushome](http://spie.org/bacushome)

### Corporate Membership Benefits include:

- 3-10 Voting Members in the SPIE General Membership, depending on tier level
- Subscription to BACUS News (monthly)
- One online SPIE Journal Subscription
- Listed as a Corporate Member in the BACUS Monthly Newsletter

[spie.org/bacushome](http://spie.org/bacushome)

## C A L E N D A R

### 2020



#### **SPIE Photomask Technology + EUV Lithography**

Free Digital Forum  
Online Only

**21-25 September 2020**

### 2021



#### **SPIE Advanced Lithography**

21-25 February 2021  
San Jose, California, USA

[www.spie.org/al](http://www.spie.org/al)



#### **Photomask Japan**

26-28 April 2021  
Yokohama, Kanagawa, Japan

[www.photomask-japan.org](http://www.photomask-japan.org)



#### **The 36th European Mask and Lithography Conference, EMLC 2021**

21-23 June 2021  
Leuven, Belgium

SPIE is the international society for optics and photonics, an educational not-for-profit organization founded in 1955 to advance light-based science and technology. The Society serves more than 255,000 constituents from 183 countries, offering conferences and their published proceedings, continuing education, books, journals, and the SPIE Digital Library in support of interdisciplinary information exchange, professional networking, and patent precedent. In 2019, SPIE provided more than \$5 million in community support including scholarships and awards, outreach and advocacy programs, travel grants, public policy, and educational resources. [spie.org](http://spie.org)

### **SPIE.**

International Headquarters  
P.O. Box 10, Bellingham, WA 98227-0010 USA  
Tel: +1 360 676 3290  
Fax: +1 360 647 1445  
[help@spie.org](mailto:help@spie.org) • [spie.org](http://spie.org)

Shipping Address  
1000 20th St., Bellingham, WA 98225-6705 USA

### **Managed by SPIE Europe**

2 Alexandra Gate, Ffordd Pengam, Cardiff,  
CF24 2SA, UK  
Tel: +44 29 2089 4747  
Fax: +44 29 2089 4750  
[spieurope@spieurope.org](mailto:spieurope@spieurope.org) • [spieurope.org](http://spieurope.org)

**You are invited to submit events of interest for this calendar. Please send to [lindad@spie.org](mailto:lindad@spie.org).**